Days *in vitro* of flow DIV	**Flow rate applied** ul/min	**Number of Transwell chips**	**Channel geometry**
5-8	0.19	4	Tapered
5-8	0.92	4	Straight
5-8	0	4	Tapered
12-15	0.19	4	Tapered
12-15	0.92	4	Tapered
12-15	0	2	Tapered
19-21	0.19	3	Tapered
19-21	0.92	3	Tapered
19-21	0	2	Tapered
26-29	0.19	3	Tapered
26-29	0.92	3	Tapered
26-29	0	2	Tapered

Table S1 Number of Transwell-chips used for each flow treatment, specifying the day *in vitro* (DIV) at which the flow was applied. Cells after DIV>10 are considered completely differentiated in agreement with [1]. Moreover, we give information about the flow rate used and the geometry of the channel. For all but one set of data we used channels with tapered geometry. Different flow rates have been used to have a wider range of shear stresses. Specifically we used $Q_1 = 0.19$ ml/min and $Q_2 = 5Q_1 = 0.92$ ml/min. For each tapered channel insert we acquired 20-25 Field of view (FOV), since the shear stress change along the main axis of the channel, the alignment parameter and the shear stress has been averaged over segment of $\delta x = 1700$ μm, that in our case correspond to 5 field of view for Transwell insert. Each field of view contains from 100 to 400 identified cells.

Journal of Experimental Biology • Supplementary information

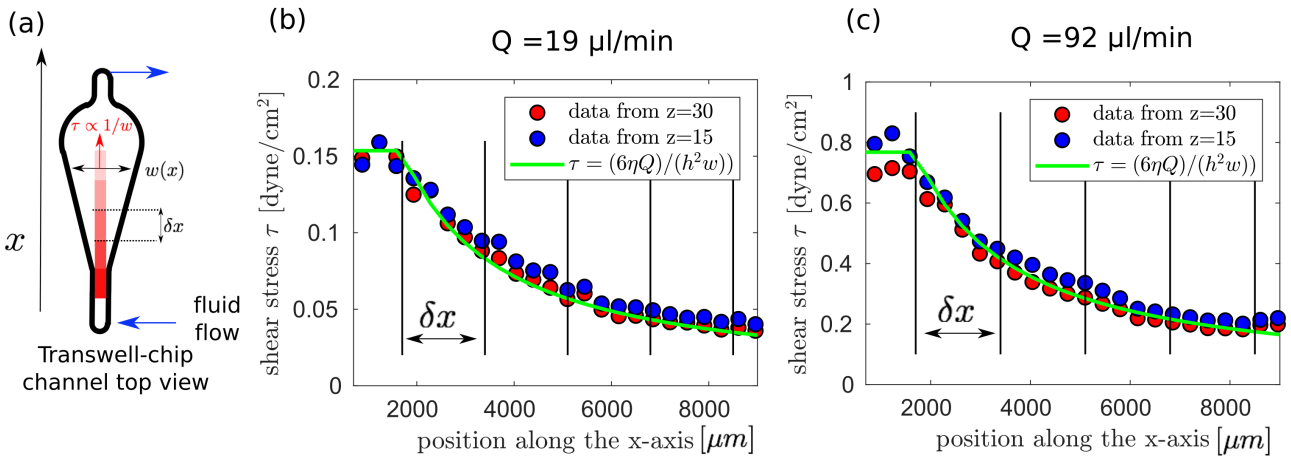

Figure S1 Shear stress measurements in taper channels. (a) Illustration of the tapered channel used to apply different shear stresses in the same cultures. The shear stress τ decreases along the main axis of the channel (x) as the channel width w increases. Since the shear stress changes continuously along the main axis of the channel, the alignment parameter and the shear stress has been averaged over segments of length $\delta x = 1700$ µm. With our equipment, we have five fields of view for each segment. (b-c) We show the shear stress τ in the tapered channel as a function of the position along the x-axis. The shear stress is measured as $\tau = \eta U(z)/z$, where z is the distance from the channel surface and $U(z)$ is the flow velocity measured at z when a flow rate Q is applied at the inlet of the tapered channel. The viscosity of the medium is $\eta = 0.8$ mPa.s. The flow velocity $U(z)$ was measured with particle image velocimetry (PIV) along the centre of the channel. For the PIV, we used polystyrene particles diameter 1 μm. We show data for flowrates $Q = 19$ μl/min and $Q = 92$ μl. We compare the trends with the shear stress expected for high aspect ratio channels.

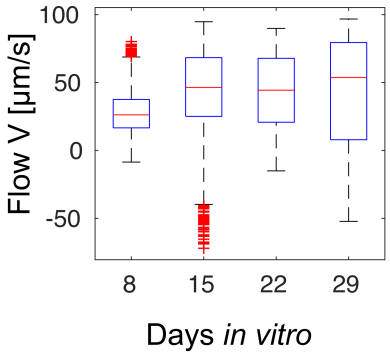

Figure S2 Global generated flow of aligned cultures. Average cilia-driven flow V in the direction of the applied shear stress as a function of the culture age (the measurement is in absence of any external flow). Data from cells treated with the highest shear stress $\tau = 0.8$ dyne/cm^2. Differentiated cells at DIV>14 propel an average fluid flow that is roughly the double of differentiating cell at DIV 8 (after shear treatment). Same dataset of Figure 2a in the main text.

Journal of Experimental Biology • Supplementary information

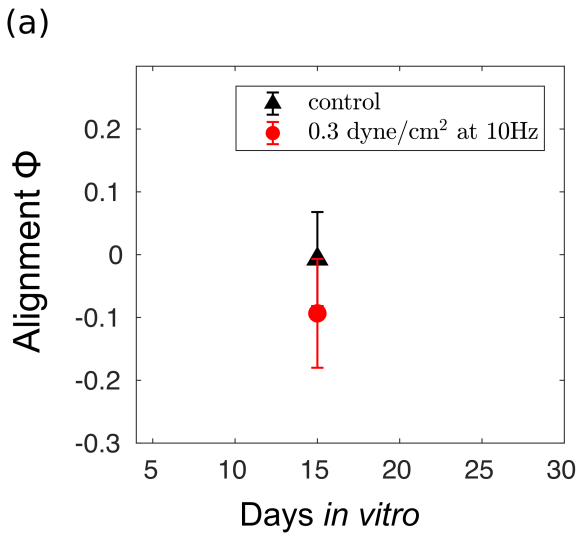

Figure S3 Cilia do not align with oscillatory flow.. Ependymal cells were exposed to oscillatory flow at DIV 15 (3 samples + control) for 3 days at average shear stress during half cycle of $\tau \approx 0.3$ dyne/cm^2. For all the samples no significant alignment was measured. For a description of the setup to create alternated flow see[2].

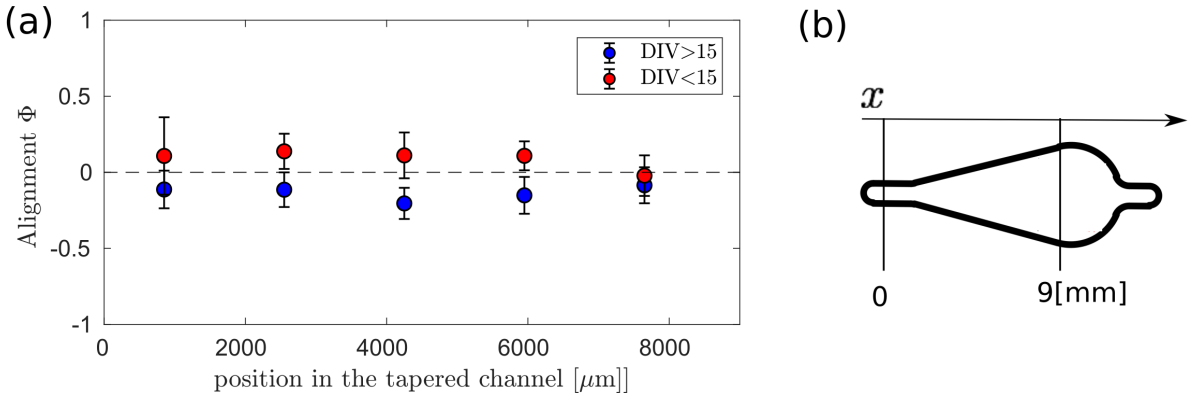

Figure S4 Cultures grown in taper channels but not treated with shear stress do not show a global alignment. a) We show the alignment parameter Φ for cells grown in tapered channels but not treated with shear stress. The alignment parameter is around zero independently on the maturation stage of the cells (DIV=8 in red or D>15 in blue) and on the position inside the tapered geometry. We used four Transwell chips for the data shown for DIV=8, and six Transwell chips for the data shown for DIV>15. Error bars are the standard error of the average. (b) An Illustration of the tapered geometry and the reference coordinates used for the graph in (a).

Journal of Experimental Biology • Supplementary information

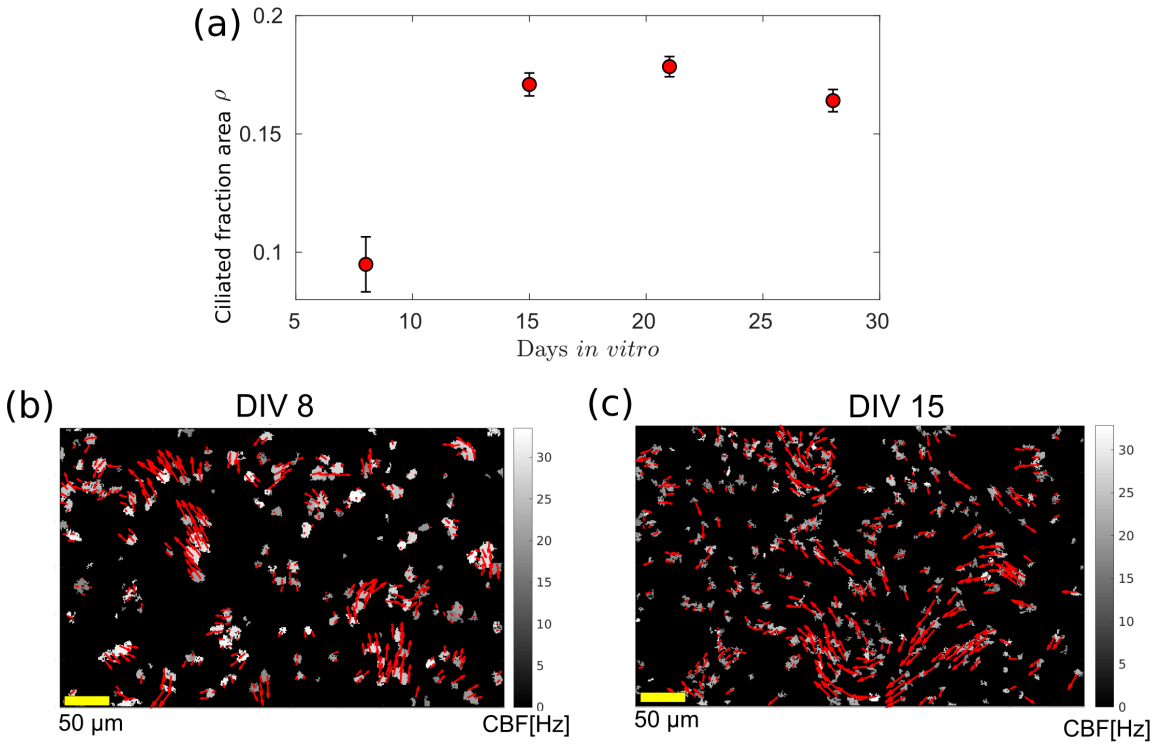

Figure S5 Ciliated fraction area increases during ependymal cell maturation. a) We show the ciliated fraction area as a function of the days *in vitro* (DIV). This number almost doubles in the period spanning from DIV 8 to DIV 15, then it flattens to approximatively the constant value of $\rho = 0.17 \pm 0.01$. Ciliated fraction area ρ is measured by the total number of boxes where ciliated cells are identified (see Methods section) for each field of view. Then the ciliated fraction area can be found by $\rho = N_{box}/N_{tot}$, where N_{box} is the number of boxes with ciliated cells and N_{tot} is the total number of boxes in a field of view. (b-c) We show examples of analysed fields of view belonging from a culture at DIV 8 (b) and DIV 15 (c), where the number of arrows correspond to the total number of identified ciliated cells. As in Figure 1, the colourmap indicates the ciliary beating frequencies (CBF) and the red arrows connote the measured flow field above the identified cells. The length of the arrows is proportional to the flow velocity.

Journal of Experimental Biology • Supplementary information

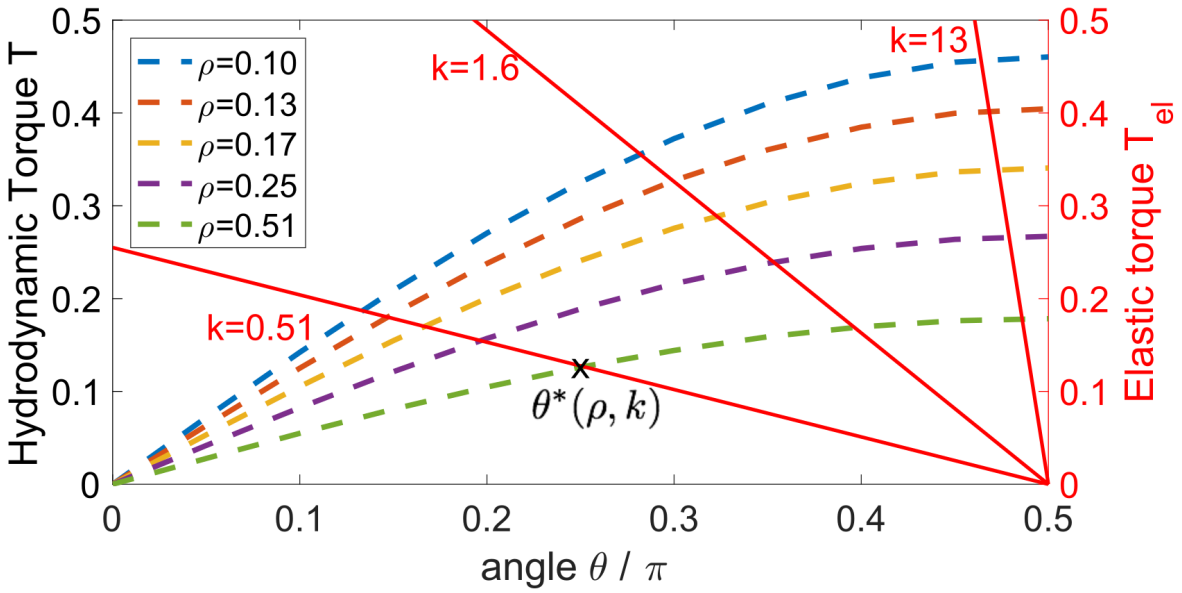

Figure S6 Modelling cilia alignment phenomena. To model the cilia alignment phenomenon, we allow the cilia beating direction to change accordingly to the hydrodynamic torque applied by the shear flow. We impose an external shear flow along the $y-$ direction. We define θ as the angle between the cilia beating direction and the external flow. In the absence of external flow, the beating direction is along the $x-$direction and $\theta = \pi/2$. In the presence of the shear flow, each individual cilium experiences a hydrodynamic drag T that drives it to rotate toward the direction of the external flow. In the figure, we reported the hydrodynamic torque on individual cilia for different values of cilia density ρ and angle θ. This torque is resisted by an effective elastic torque acting at the base of the ciliary array. This elastic torque is modelled as a torsional spring that is a linear function of ϕ: $T_{\mathrm{el}} = k(\pi/2 - \theta)$, where k is the effective spring stiffness. In the figure, we plot the elastic torques for three values of k as a function of θ. The beating direction rotates toward the direction of the shear flow until an equilibrium angle $\theta = \theta^*$ is reached - when the hydrodynamic torque acting on the cilium balances the elastic torque arising from the base. The equilibrium angle θ^* is reached when the red straight lines (representing the elastic torque) intercept the hydrodynamic torque curves. In the figure, we marked (with a cross) the equilibrium angle θ^* for an array of cilia with density $\rho = 0.51$ and effective spring stiffness $k = 0.51$. The equilibrium angle θ^* leads to the alignment parameter$\Phi = \cos(\theta^*)$.

Journal of Experimental Biology • Supplementary information

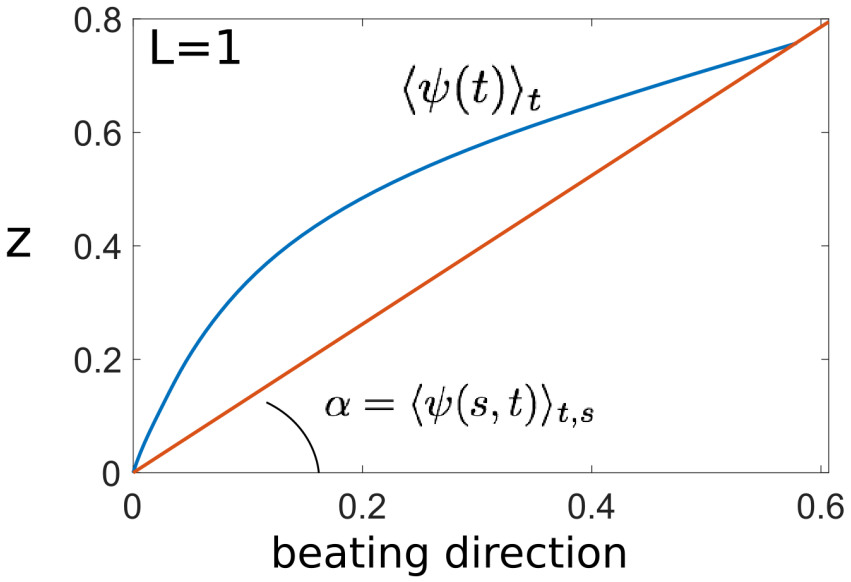

Figure S7 Additional information on the corse-graining of the cilium beating pattern. The beat pattern of a single cilium from ependymal culture, data taken from ref.[3], is taken as an input. The cilium centreline is characterised by its tangent profile(s,t) as a function of the arclength along the cilium s and at the time t. The blue line represents the average over time (one period) of the cilium centerlines $\langle(s,t)\rangle_t$. from this we can find the average angle $\langle(s,t)\rangle_{t,s} = \alpha = 53°$ of the cilium with respect to the direction of the power stroke. Both lines have normalised arclengths $L = 1$. All the hydrodynamics screening calculations reported in the main text were performed using the red line as an approximation of the cilium beating pattern. It is worth noting that the value of the torque applied by a shear flow could depend on the choice of the cilium corse-graining. Below we report the values of the torques, T, on an individual cilium using different approximations for the cilium itself. We report the values only for the case when the shear flow is perpendicular to the cilia beating plane ($\theta = \pi/2$), i.e, when shear flow is into the y-plane while the cilia beats in the x-z plane. A) Torque on the average beating pattern over time (one period), Blue line, $T = 0.29$; B) Torque on the filament at the angle $\langle(s,t)\rangle_{t,s} = \alpha = 53°$, Red line $T = 0.55$; C) Average of the torques over all cilia positions (see Figure 4a), $T = 0.17$. These values are non-dimensionalised by $\eta\dot{\gamma}L^3$, where $\dot{\gamma}$ is the dimensionless shear rate, η is the viscosity and L the cilium length.

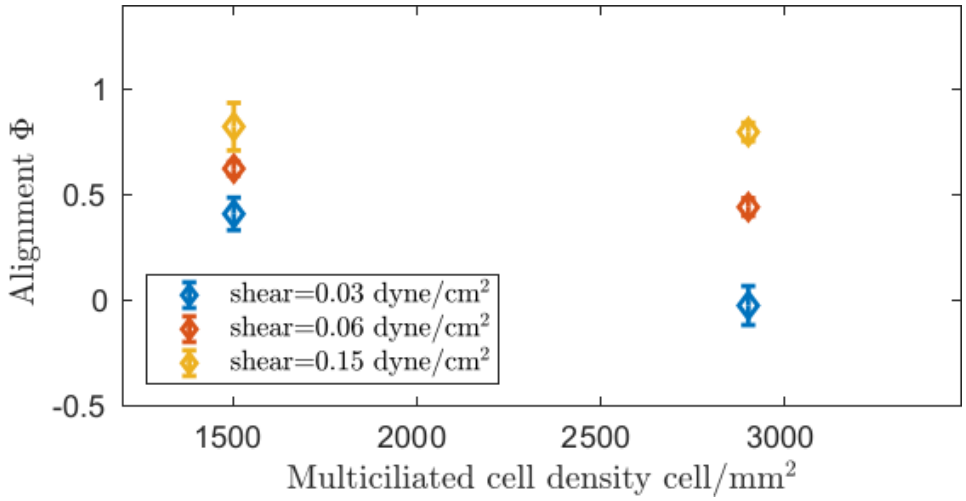

Figure S8 Cilia alignment depends on the density of multiciliated cells. Here we report the alignment parameterΦ as a function of the density of multiciliated cells during the maturation period. The data reported for the cultures with higher density of cilia is the one for cultures with DIV≥15 already provided in the main text in the Figure3b. On the other hand the data for cultures with low cell density are the one for cultures at DIV=8, already reported in Figure 3a. The decrease of alignment with cell density is clear when low shear stress are applied (blue markers). The gap between the two values is flattened for higher shear stress, when both the alignment parameters are saturating to one. We choose to show these data as a function of the multiciliated cell density. However, it is worth noting that the density of multiciliated cells is, in our approximation, also proportional to the ciliated fraction area.

References

[1] Boris Guirao, Alice Meunier, Stéphane Mortaud, Andrea Aguilar, Jean-Marc Corsi, Laetitia Strehl, Yuki Hirota, Angélique Desoeuvre, Camille Boutin, Young-Goo Han, Zaman Mirzadeh, Harold Cremer, Mireille Montcouquiol,

Journal of Experimental Biology • Supplementary information

Kazunobu Sawamoto, and Nathalie Spassky. Coupling between hydrodynamic forces and planar cell polarity orients mammalian motile cilia. *Nature Cell Biol.*, 12:341–350, 2010.

[2] Nicola Pellicciotta, Evelyn Hamilton, Jurij Kotar, Marion Faucourt, Nathalie Degehyr, Nathalie Spassky, and Pietro Cicuta. Entrainment of mammalian motile cilia in the brain with hydrodynamic forces. *Proc. Natl. Acad. Sci. USA*, 2020.

[3] Evelyn Hamilton, Nicola Pellicciotta, Luigi Feriani, and Pietro Cicuta. Motile cilia hydrodynamics: entrainment versus synchronization when coupling through flow. *Philos. Trans. R. Soc. B*, 375(1792):20190152, 2020.

Journal of Experimental Biology • Supplementary information

Movie 1

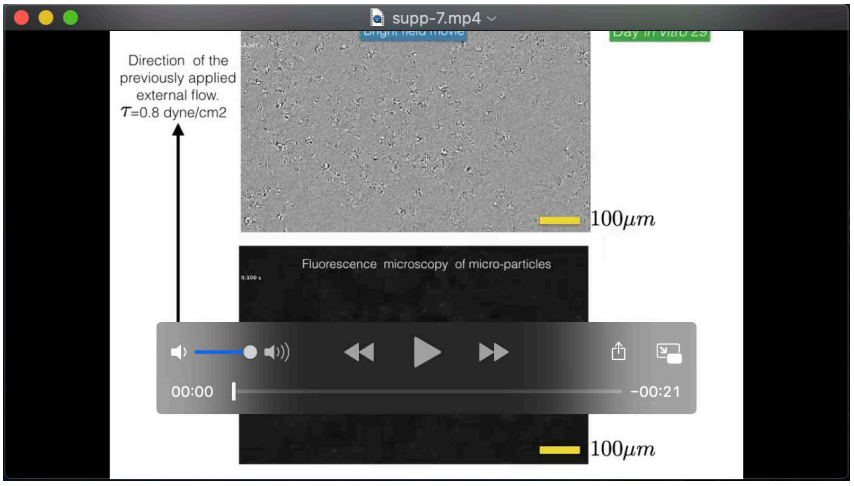

Movie 2

Journal of Experimental Biology • Supplementary information